Journal of Controlled Release 186 (2014) 1–10

Contents lists available at ScienceDirect

Journal of Controlled Release

journal homepage: www.elsevier.com/locate/jconrel

In vivo near-infrared fluorescence imaging of FAP-expressing tumors with activatable FAP-targeted, single-chain Fv-immunoliposomes

Ronny Rüger [a,*,1], Felista L. Tansi [b,**,1], Markus Rabenhold [a], Frank Steiniger [c], Roland E. Kontermann [d], Alfred Fahr [a,*], Ingrid Hilger [b,**]

[a] Department of Pharmaceutical Technology, Friedrich-Schiller-University Jena, Lessingstrasse 8, 07743 Jena, Germany
[b] Dept. of Experimental Radiology, Institute of Diagnostic and Interventional Radiology I, Jena University Hospital-Friedrich Schiller University Jena, Erlanger Allee 101, 07747 Jena, Germany
[c] Center for Electron Microscopy, Jena University Hospital-Friedrich Schiller University Jena, Ziegelmuehlenweg 1, 07743 Jena, Germany
[d] Institute of Cell Biology and Immunology, University Stuttgart, Allmandring 31, 70569 Stuttgart, Germany

ARTICLE INFO

Article history:
Received 23 December 2013
Accepted 24 April 2014
Available online 5 May 2014

Keywords:
FAP
Immunoliposomes
Fluorescence-quenching
NIRF
Optical imaging

ABSTRACT

Molecular and cellular changes that precede the invasive growth of solid tumors include the release of proteolytic enzymes and peptides in the tumor stroma, the recruitment of phagocytic and lymphoid infiltrates and alteration of the extracellular matrix. The reactive tumor stroma consists of a large number of myofibroblasts, characterized by high expression of fibroblast activation protein alpha (FAP). FAP, a type-II transmembrane sialoglycoprotein is an attractive target in diagnosis and therapy of several pathologic disorders especially cancer. In the underlying work, a fluorescence-activatable liposome (fluorescence-quenched during circulation and fluorescence activation upon cellular uptake), bearing specific single-chain Fv fragments directed against FAP (scFv′FAP) was developed, and its potential for use in fluorescence diagnostic imaging of FAP-expressing tumor cells was evaluated by whole body fluorescence imaging. The liposomes termed anti-FAP-IL were prepared via post-insertion of ligand–phospholipid-conjugates into preformed DY-676-COOH-containing liposomes. The anti-FAP-IL revealed a homogeneous size distribution and showed specific interaction and binding with FAP-expressing cells *in vitro*. The high level of fluorescence quenching of the near-infrared fluorescent dye sequestered in the aqueous interior of the liposomes enables fluorescence imaging exclusively upon uptake and degradation by cells, which results in fluorescence activation. Only FAP-expressing cells were able to take up and activate fluorescence of anti-FAP-IL *in vitro*. Furthermore, anti-FAP-IL accumulated selectively in FAP-expressing xenograft models *in vivo*, as demonstrated by blocking experiments using free scFv′FAP. The local tumor fluorescence intensities were in agreement with the intrinsic degree of FAP-expression in different xenograft models. Thus, anti-FAP-IL can serve as a suitable *in vivo* diagnostic tool for pathological disorders accompanied by high FAP-expression.
© 2014 Elsevier B.V. All rights reserved.

1. Introduction

A crucial step towards defining a correct personalized anticancer therapy is the identification of the genes and pathways altered in the tumor of the patient. In this respect a significant number of studies have revealed fibroblast activation protein alpha (FAP), as a promising tumor target for designing novel pharmaceuticals for both cancer diagnosis and therapy [1]. FAP is a type-II transmembrane sialoglycoprotein and a member of the conserved family of serine proteases which are capable of cleaving the post-prolyl bond of peptides and proteins [2]. FAP is selectively expressed by tumor-associated fibroblasts in over 90% of malignant breast, colorectal, skin, and pancreatic tumors, but not in normal adult tissues [3–5]. Opposed to its protease family members, FAP possesses an additional gelatinase activity [6,7]. Due to these properties, FAP serves as a biomarker of cancer-associated fibroblasts (CAFs) in the tumor stroma, where it modulates proliferation, invasion and metastasis [8–10]. Thus, FAP has been considered as a target in several preclinical approaches and clinical trials. For example a humanized anti-FAP monoclonal antibody (sibrotuzumab) revealed safety and dose tolerance after repeated administrations in phase II clinical trials [11].

Considering that, FAP plays a central role in the invasiveness of solid tumors and given that 90% of the stromal fibroblasts of many cancer types express the protein, the development of diagnostic approaches by targeting FAP would be of great importance. *In vivo* optical imaging using near infrared (NIR) fluorescent probes is a non-invasive approach that exploits the fact that biological tissues show very low absorption and auto-fluorescence in the NIR spectrum window [12]. The potential of this approach in diagnostic and intraoperative imaging and in the monitoring of treatment response has been repeatedly demonstrated [13–15]. Thus, molecular imaging probes bearing peptide ligands or

* Corresponding authors. Tel.: +49 3641 949905.
** Corresponding authors.
E-mail addresses: ronny.rueger@uni-jena.de (R. Rüger), felista.tansi@med.uni-jena.de (F.L. Tansi), alfred.fahr@uni-jena.de (A. Fahr), ingrid.hilger@med.uni-jena.de (I. Hilger).
[1] Contributed equally to this work.

http://dx.doi.org/10.1016/j.jconrel.2014.04.050
0168-3659/© 2014 Elsevier B.V. All rights reserved.

antibodies directed towards FAP would enable classification of cancer patients for FAP-targeted therapy. So far, FAP-targeted probes that serve as non-invasive imaging tools for early detection of cancer have mostly been reported in *in vitro* studies [16–18]. In an *in vivo* approach to target FAP in optical imaging the covalent coupling of the NIRF dye Cy5.5 to a restriction peptide sequence for FAP was used [19].

However, this approach only detects enzymatically active FAP whereas modified forms of the protein expressed on tumor cells would not be addressed. Furthermore, there are some drawbacks using protein and peptide-based molecular imaging probes. The amount of fluorescent molecules per ligand is limited to a defined number per ligand [20]. Increasing the number of imaging molecules per ligand without reaching a quenching concentration increases the background signal during circulation [21]. Non-site directed conjugation processes used for labeling of *e.g.* antibodies can reduce the binding activity of the ligand to the target due to the induced conformational changes or physically blocking the antigen binding sites [22]. Furthermore, the smaller the ligands the lower is their blood circulation half-life. Due to their small size and the lack of recycling processes mediated by the neonatal Fc receptor (FcRn) for whole antibodies, ligands such as peptides, scFv, diabodies and single-chain diabodies are quickly cleared by renal filtration [23,24].

To circumvent these drawbacks, we developed an immunoliposome-based NIRF-FAP-imaging probe for *in vivo* application. The use of liposomes is advantageous in terms of high cargo payload and biocompatibility [25,26]. Although, the intravenous administration of nanoparticle formulations such as the clinical doxorubicin-containing, PEGylated liposome, Doxil can induce immunological reactions such as liposomal complement activation-related pseudoallergy (CARPA) [27–30], premedication with Doxil-like empty liposomes (Doxebo) and a slow infusion showed improved tolerance to Doxil [31] supporting their potential as suitable drug delivery vesicles. Recently, we demonstrated that non-targeted, PEGylated liposomes can be selectively taken up by phagocytosis and activated in phagolysosomes thereby enhancing the imaging of inflammatory areas *in vivo* [32]. The use of liposomes circumvents the rapid clearance seen with peptide and antibody fragment-based probes alone and enables the combination of imaging with therapy.

Here we sought to address the FAP in tumors by utilization of target-affine fluorescence activatable liposomes. The use of a scFv as binding moiety ensures specific binding to the target and at the same time reduces possible adverse immune responses that may result from applying whole antibodies [33]. We evaluated whether covalent linkage of scFv′FAP at the surface of fluorescence-activatable liposomes will enable FAP-targeted delivery of fluorescent dyes in FAP-expressing tumors *in vivo*, thereby enhancing molecular imaging of FAP-expressing tumor models in mice. We demonstrate that specific uptake and activation of anti-FAP-IL take place exclusively in FAP-expressing cells *in vitro*. Furthermore, the uptake and activation of anti-FAP-IL by FAP-expressing tumor cells enhanced whole body *in vivo* near-infrared fluorescence imaging of xenograft models in mice. Hence, anti-FAP-IL can be used to predict prognosis, guide intraoperative treatment and monitor treatment success.

2. Abbreviations

FAP	fibroblast activation protein-alpha;
NIR	near-infrared;
p.i	post injection;
ROI	regions of interest
scFv	single-chain Fv fragment

3. Materials and methods

3.1. Materials

Egg phosphatidylcholine (EPC) was purchased from Lipoid (Ludwigshafen, Germany); cholesterol, Tris(hydroxymethyl)-aminomethane (Tris), 2-(4-(2-hydroxyethyl)-1-piperazinyl)-ethansulfonsäure (HEPES) and 4-(1,1,3,3-tetramethylbutyl)phenyl-polyethylene glycol (Triton-X100) were purchased from Sigma (Taufkirchen, Germany); and 1,2-distearoyl-sn-glycero-3-phosphoethanolamine-N-[methoxy (polyethylene glycol)-2000] (ammonium salt) ($mPEG_{2000}$-DSPE), 1,2-distearoyl-sn-glycero-3-phosphoethanolamine-N-[maleimide (polyethylene glycol)-2000] (ammonium salt) ($MalPEG_{2000}$-DSPE) and 1,2-dioleoyl-sn-glycero-3-phosphoethanolamine-N-(7-nitro-2-1,3-benzoxadiazol-4-yl) (ammonium salt) (NBD-DOPE) were purchased from Avanti Polar Lipids (Alabaster, USA). The free acid of the near infrared fluorescent dye DY-676-COOH and DY-676-maleimide was purchased from Dyomics GmbH (Jena, Germany).

3.2. Preparation of quenched DY-676-COOH containing liposomes (Lip-Q)

All liposomes were prepared by the film hydration and extrusion method [34]. Vesicles were composed of EPC:Chol:$mPEG_{2000}$-DSPE at a molar ratio of 6.5:3:0.5. Anti-FAP-IL used for plasma stability experiments were stained with 0.3 mol% of the lipophilic, red fluorescent 1,1′-dioctadecyl-3,3,3′,3′-tetramethylindocarbocyanine perchlorate (Sigma-Aldrich, Taufkirchen, Germany). Double stained liposomes were prepared whereby the hydrophilic DY-676-COOH was encapsulated within the liposomes and the lipophilic liposome-membrane marker NBD-DOPE (0.3 mol.%) was incorporated into the liposomal phospholipid bilayer. 100 μmol (100 mM) lipid was hydrated by using DY-676-COOH (6.18 mM) dissolved in 10 mM Tris buffer, pH 7.4. Subsequently, the dispersions were frozen in liquid nitrogen and thawn at room temperature seven times [32]. The resulting vesicle dispersions were homogenized via hand extrusion, 21 times through a 100 nm polycarbonate membrane, using a LiposoFast-Basic extruder (Avestin, Ottawa, Canada). A subsequent gel filtration via a self-prepared Sephadex G25 column (length 26 cm, diameter 0.8 cm) was accomplished to purify DY-676-COOH containing liposomes from non-encapsulated, free DY-676-COOH. Due to dilution during gel filtration the DY-676-COOH containing liposomes were centrifuged (2 h, 100,000 *g*, 8 °C) using a Beckman XL80 equipped with rotor SW55-Ti (Beckman Coulter GmbH, Krefeld, Germany) to concentrate the samples. This procedure results in 100 μmol plain liposomes filled with DY-676-COOH (Lip-Q), assuming no lipid loss during preparation.

3.3. Preparation and purification of single-chain Fv fragments directed against FAP

The scFv′FAP were produced in *Escherichia coli (E. coli)* by periplasmic preparation and purified via immobilized metal affinity chromatography (IMAC) [34]. The protein concentration was determined by measuring the absorbance at 280 nm. The scFv fragments were analyzed via sodium dodecyl sulfate polyacrylamide gel electrophoresis (SDS-PAGE according to Laemmli) 12% under reducing and non-reducing conditions and stained with Coomassie brilliant blue G250 (Carl Roth GmbH, Karlsruhe, Germany).

3.4. Preparation of anti-FAP-immunoliposomes and scFv′FAP-DY-676 conjugates

Plain DY-676-COOH containing liposomes (100 μmol, Lip-Q) were divided into two halves. The first half (50 μmol lipid) was used for the post-insertion with 0.1 mol.% cysteine-conjugated $MalPEG_{2000}$-DSPE micelles as control (meaning 50 nmol $MalPEG_{2000}$-DSPE anchor lipid) and the second half was used for the post-insertion with 0.1 mol.% $MalPEG_{2000}$-DSPE micelles conjugated to scFv′FAP. The ligand–micelle conjugates were inserted into preformed PEGylated liposomes as described elsewhere [17]. Mal-PEG_{2000}-DSPE micelles were prepared and conjugated with reduced ligands (scFv′FAP or cysteine) according to literature [35] with slight differences.

Coupling reaction between scFv′FAP and thioreactive micelles was performed at room temperature for 60 min. The coupling efficiency

was analyzed by SDS-PAGE and evaluated using the freeware ImageJ version 1.45 s. The scFv′FAP-coupled $MalPEG_{2000}$-DSPE micelles were inserted into preformed PEGylated liposomes by incubation at 50 °C in a water bath for 30 min. Unbound scFv molecules were removed by gel-filtration using a Sepharose CL4B column (Amersham, Braunschweig, Germany). The liposomes were centrifuged (2 h, 100,000 *g*, 8 °C) using a Beckman XL80 equipped with a SW55Ti rotor and re-suspended in 1 ml sterile Tris buffer (10 mM, pH 7.4). To directly label scFv′FAP fragments with DY-676 molecules, the scFv′FAP was reduced and dialysed as above. The reduced scFv′FAP was incubated with a 10 fold molar excess of the thioreactive DY-676-maleimide derivative for 60 min at room temperature. Afterwards, the resulting scFv′FAP-DY-676 was washed up to 30 times using a Microcon® centrifugal filter device with a 3000 Da molecular weight cut off.

3.5. Characterization of liposomes

Sizes of liposomes were measured via dynamic light scattering and the zeta potential was determined by using a Zetasizer Nano ZS (Malvern, Herrenberg, Germany).

3.6. Cryo-transmission electron microscopy

Approximately 20 μl of the liposome dispersion was applied to a copper grid covered by holey carbon film Quantifoil R3.5/1 (Micro Tools GmbH, Jena, Germany). Excess of liquid was blotted automatically for 3 s between two strips of filter paper. Subsequently, the samples were rapidly plunged into liquid ethane (cooled to about −180 °C) in a cryobox (Carl Zeiss NTS GmbH, Oberkochen, Germany). Excess ethane was removed with a piece of filter paper. The samples were transferred with a cryo-transfer unit (Gatan 626-DH) into the pre-cooled cryo-transmission electron microscope Philips CM 120 (Philips Research, Eindhoven, The Netherlands) operated at 120 kV and viewed under low dose conditions. The images were recorded with a 1 K CCD Camera FastScan F114 (TVIPS, Gauting, Germany).

3.7. Quantitation of liposomal encapsulated DY-676-COOH

To quantify the amount of DY-676-COOH encapsulated, a calibration curve was prepared by dissolving DY-676-COOH (0, 82, 124, 247, 494, 741, 988 nM) in 10 mM Tris buffer, pH 7.4 containing 0.1% Triton X100. The liposome samples were incubated 5 min at RT in presence of 1% Triton X100 and afterwards diluted with 10 mM Tris buffer, pH 7.4 to a final Triton-X100 concentration of 0.1%. All samples were measured in triplicates on a Fluostar Optima microplate reader (BMG Labtech, GmbH, Ortenberg, Germany) equipped with adequate filters for excitation at $\lambda = 645$ nm and measuring the emitted fluorescence light at $\lambda = 700$ nm. The quantitation of DY-676-COOH was performed with the final liposomal formulations (Cys-Lip/anti-FAP-Lip).

3.8. Liposomal quenching assay

The fluorescence-quenching and activation effect of anti-FAP-IL and Lip-Q was analyzed *in vitro*, by measuring the fluorescence intensity before and after liposomal freeze-damaging as described earlier [32].

3.9. Cell lines

The human melanoma cell line, MDA-MB435S was purchased from the Cell Lines Service, (CLS, Heidelberg, Germany). The fibrosarcoma cell line, HT1080 and its FAP-transfected counterparts HT1080-hFAP (human FAP) and HT1080-mFAP (murine FAP), SKBR3, B16F10, HEK293 were cultured in a RPMI medium supplemented with 5% (*v*/*v*) fetal calf serum (both Life Technologies GmbH, Darmstadt, Germany) whereas the MDA-MB435S cells were grown in Dulbecco's modified Eagle's medium containing 10% FCS and 1% HEPES. Human umbilical vein endothelial cells (HUVECs) were isolated from human umbilical vein and cultured in Endothelial cell Growth Medium (ECGM) (Promocell, Germany). The cells were grown at 37 °C in a 5% CO_2 and 95% humidified atmosphere.

3.10. Flow cytometry

To analyze the interaction of anti-FAP-IL with FAP-expressing cells, 0.5×10^6 HT1080-mFAP in 100 μl RPMI (5% FCS) were incubated with liposomes (496 μM, 1 h, on ice, in the dark). For competition experiments the cells were simultaneously incubated with anti-FAP-IL and 10 μg free scFv′FAP under the same conditions as described above. This reflects a nearly 40 fold excess of free scFv′FAP over liposomal bound scFv′FAP. After incubation, cells were washed three times with 3 ml PBA (PBS, 2% FCS, 0.02% sodium azide), re-suspended in 450 μl PBA and analyzed using an Epics XL-MCL (Beckmann Coulter, Krefeld, Germany). Data were evaluated using the freeware WinMDI 2.9.

3.11. Plasma stability experiments

Anti-FAP-IL was incubated with equal volumes of PBS or human plasma (Institute of Transfusion Medicine, University Hospital, Jena, Germany) for 24 h at 37 °C. Afterwards, the indicated amount of anti-FAP-IL was incubated with HT1080-mFAP cells for 1 h at 4 °C. The cells were then analyzed by flow cytometry as afore mentioned. For long term investigation (Supporting Information S5) liposomes were pre-treated with human plasma and PBS at 37 °C for up to 72 h.

3.12. Uptake of liposomal probes and imaging

For confocal microscopy, 30,000 cells (HT-1080, HT1080-hFAP, MDA-MB435S) were grown on poly-L-lysine-coated 8-well culture slides (BD Biosciences) for 16 h. Afterwards, 200 nmol (final lipid) of the liposomes was added and the cells were further cultured for 6–8 h at 37 °C or 4 °C. For time-course comparison of anti-FAP-IL and free scFv′FAP-DY-676 uptake, the HT-1080 and HT1080-hFAP cells were prepared in small culture flasks (2.0×10^6 cells) or on coated chamber slides (30,000 cells) then treated with anti-FAP-IL (100 nmol final lipid) or 2 μg scFv′FAP-DY-676 for 4 h, 8 h, 12 h and 24 h. The cells were washed 3 times with HBSS and fixed with 3.7% (*v*/*v*) formaldehyde (Roth, Karlsruhe, Germany) in PBS for 30 min at RT. Cells in culture flasks were scraped in 500 μl HBSS and pelleted by centrifugation and imaged in the Maestro™ *in vivo* fluorescence imaging system and signal intensities quantified (as described under "*in vivo* near-infrared fluorescence imaging" below). The cells were washed twice with PBS, mounted with PermaFluor (Thermo Fisher Scientific GmbH, Schwerte, Germany) containing the DNA stain Hoechst-33258 (Applichem GmbH, Darmstadt, Germany) then covered with glass cover-slips and subsequently imaged on the LSM510-META confocal microscope (Zeiss, Jena, Germany). The nuclei were visualized with a 405 nm laser diode and a 420–480 nm bandpass filter. A 543 nm HeNe laser and a 550–615 nm band pass filter were applied, whereby fluorescence of DY-676-COOH was excited with a 633 nm argon laser and emission was detected with a 650 nm longpass filter. Fluorescence emission of NBD-DOPE was detected with the GFP filter at 530 nm after excitation at 488 nm.

3.13. Animals and implantation

All procedures were approved by the regional animal committee and were in accordance with international guidelines on the ethical use of animals. 10–14 week-old female athymic nude mice ($n = 55$; Hsd:Athymic Nude-Foxn1^{nu} nu/nu; Harlan Laboratories) weighing approximately 20 g were housed under standard conditions with food and water *ad libitum*. 14–21 days prior to *in vivo* imaging, xenografts were induced by implanting 1.0×10^6 cells (HT1080-wt), 1.5×10^6 cells (HT1080-hFAP) or 2.0×10^6 cells (MDA-MB435S) subcutaneously.

Briefly, the cells were pelleted and dispensed in 100 μl cold Matrigel™ (BD Biosciences, Heidelberg, Germany) then injected subcutaneously into the lower back of the mice. Seven days prior to probe injection and imaging, all mice received a low pheophorbide diet C1039 (Altromin Spezialfutter GmbH & Co. KG, Lange, Germany) in order to reduce tissue auto-fluorescence. Throughout all procedures, animals were anesthetized with 2% isoflurane.

3.14. In vivo near-infrared fluorescence imaging

Mice bearing subcutaneous xenografts with approximate diameters of 5–9 mm (with average tumor volume of 138 mm^3 for HT1080-wt, 66 mm^3 for HT1080-hFAP and 32 mm^3 for MDA-MB435S) were anaesthetized with 2% isoflurane and the respective liposomal solutions (30 μmol (lipid)/kg weight) applied intravenously through the tail vein. To control for signal specificity and contribution of EPR effect, a group of the animals received liposomal probe together with 10 μg free scFv′FAP (which is comparable to 8.15 μg liposomal scFv′FAP in anti-FAP-IL) or only the free scFv′FAP-DY-676, which was covalently coupled to DY-676-maleimide (Supporting Information S6). The animals were immediately imaged with the Maestro™ *in vivo* fluorescence imaging system (Maestro™, CRi Woburn, UK) by exciting with filters for the excitation range 615–665 nm and acquiring emission with a cut-in filter (>700 nm) and recordings made as time point, $t = 0$ h post injection (p.i.). The animals were further imaged every 2 h for 10 h and again at $t = 24$ h–32 h and at 48 h p.i. The evaluation and extraction of background auto-fluorescence of native animals were performed with the Maestro™-software according to the manufacturer's instructions. Semi-quantitative analysis of fluorescence intensities of tumors was acquired by assigning a region of interest (ROI) to each tumor (target) and another on the hind leg region of the animals (muscle/skin = background). Fluorescence intensities were deduced as average signal (scaled counts/s). This represents count levels after scaling for exposure time, camera gain, binning and bit depth, and makes the measurements comparable among each other.

3.15. Ex vivo determination of the biodistribution of anti-FAP-IL

48 h post contrast agent injection and imaging, the animals were sacrificed and the organs and tumors were imaged. Semi-quantitative determination of the respective fluorescence intensities was performed with the Maestro™ imaging system as described above.

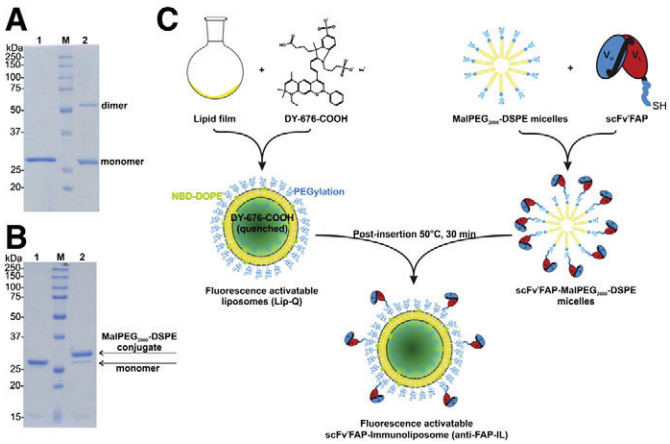

Fig. 1. Analysis of scFv′FAP by 12% SDS-PAGE: A.) 2 μg of purified scFv′FAP under reducing (1) and non-reducing conditions (2). B.) The scFv′FAP analyzed under non-reducing conditions before (1) and after (2) conjugation to $MalPEG_{2000}$-DSPE micelles. C.) Schematic overview of the preparation of anti-FAP-IL.

3.16. Immunohistochemistry

After imaging, mice were euthanized and tumors were collected, fixed in methanol-stabilized 5% formaldehyde solution (Otto-Fischar GmbH, Saarbrücken, Germany) for 24 h at 4 °C, then embedded in paraffin. Using a microtome system (Microm HM 340E) (Thermo-Fisher Scientific GmbH, Schwerte, Germany), three-micron thick serial sections of the samples were cut, mounted on (poly-L-lysin)-coated glass slides and air-dried. The paraffin-embedded sections were dewaxed, and antigen retrieval was performed in 10 mM sodium citrate buffer, pH 7.4, for 20 min at 95 °C. Slides were washed three times in TBS-T (containing 1% Tween 20) at RT and hydrated in PBS for 10 min. Blocking for unspecific receptor binding was performed with 1% BSA and 0.1% Tween-20 in PBS pH 7.4, for 1 h at RT. Thereafter, the slides were washed 2 times with PBS for 5 min each. Tissue sections were incubated overnight at 4 °C with anti-alpha-smooth muscle actin primary antibody (anti-αSMA mAb, A2547, Sigma Aldrich, Taufkirchen, Germany) in order to detect stromal fibroblasts. This was followed by a 3 times washing step and incubation with Alexa-Fluor-488-coupled goat anti-mouse IgG, (aza11029, Mobitec GmbH, Goettingen, Germany) for 30 min at RT. The sections were washed 3 times, mounted with Permafluor (Applichem GmbH, Darmstadt, Germany) containing a 1:50 dilution of the DNA stain Hoechst-33258 and then cover slipped. Fluorescence images were acquired using the Zeiss LSM510-META confocal laser scanning microscope as indicated for *in vitro* uptake experiments.

3.17. Statistical data

Except otherwise indicated, Student's *t*-test was used to deduce the level of significance, if normality and equal variance tests were passed. Else Mann–Whitney-Rank sum test was applied. All experiments were done at least in duplicates. *In vivo* animal trials were performed with 4 or more animals/group. Differences resulting in $P < 0.05$ were considered significant.

4. Results

4.1. Preparation of FAP-specific scFv and fluorescence-activatable scFv-immunoliposomes

The FAP-specific single-chain Fv fragments (scFv′FAP) purified from *E. coli* contained a distal sulfhydryl group for a site-directed conjugation to thioreactive groups. The yield was 0.35 mg per liter bacteria suspension. The scFv′ showed a characteristic monomer band under reducing conditions (Fig. 1A, lane 1) and formed approximately 27.5% disulfide-linked dimers under non-reducing conditions (Fig. 1A, lane 2). The reduced scFv′FAP was conjugated covalently to micelles composed of Mal-PEG_{2000}-DSPE via thioether linkage. SDS-PAGE revealed a coupling efficiency of approximately 88% (Fig. 1B). The anti-FAP-IL was then prepared via post-insertion of 0.1 mol.% scFv′FAP-$MalPEG_{2000}$-DSPE conjugates into activatable fluorescent liposomes (Lip-Q) [32] which were prepared with high quenching concentrations of the NIRF dye, DY-676-COOH in the aqueous interior and the green fluorescent phospholipid NBD-DOPE on the lipid interface (Fig. 1C). Cys-Lip were prepared as control liposomes by coupling of $MalPEG_{2000}$-DSPE micelles to L-cysteine. L-cystein-$MalPEG_{2000}$-DSPE micelles were post-inserted into plain liposomes (Lip-Q).

4.2. Characterization of activatable scFv-targeted immunoliposomes

Different liposomal formulations were prepared and compared. The Z-averages of all the liposomal formulations were below 160 nm with polydispersity indices (PDI) below 0.1 (Table 1). These data were further confirmed by cryo-electron microscopy (Fig. 2A). Most of the vesicles in Lip-Q (before post-insertion) as well as Cys-Lip and anti-FAP-IL

Table 1
Characterization of liposomes by dynamic light scattering.

Liposome	Size [nm]	Polydispersity index (PDI)	Zeta potential [mV]	$C_{Dy676\text{-}COOH}$ [μg/ml]	C_{Lipid} [mM]
Cys-Lip	126 ± 5.1	0.069 ± 0.03	−13.9 ± 6.7	135.2 ± 21.5	50
Anti-FAP-IL	139.1 ± 25	0.079 ± 0.02	−15.4 ± 4.9	148.6 ± 5	50
Lip-Q	118.5 ± 0.7	0.04 ± 0.02	−9 ± 2	68.76 ± 5.9	21

(after post-insertion) were unilamellar with less than 42% bilamellar structures and exhibited a vesicular morphology.

The fluorescence-activatable liposomes retained their fluorescence quenching effect even after insertion of the scFv′FAP-MalPEG$_{2000}$-DSPE conjugates. This could be detected in a double absorption peak of the anti-FAP-IL (Fig. 2B, anti-FAP-IL—bold line) which was comparable to that seen with the liposomes prior to insertion (Fig. 2B, LipQ—bold line). Following rupturing of the anti-FAP-IL by harsh freezing at −80 °C and thawing at 30 °C, an increase in the absorption maximum and the disappearance of the blue-shifted peak was observed (Fig. 2B, broken lines). This revealed fluorescence quenching of the encapsulated DY-676-COOH, which was not altered by the scFv′ insertion performed above the liposomal phase transition temperature.

4.3. Specificity of liposomal uptake by FAP-expressing cells

To verify the binding specificity of double-labeled anti-FAP-IL, the stable transfected human fibrosarcoma cell line HT1080-mFAP was incubated with different liposomal formulations and analyzed by flow cytometry with the aid of the green fluorescent phospholipid NBD-DOPE localized in the liposomal membrane. Whereas specific binding of anti-FAP-IL to the FAP-expressing cells was detected, (Fig. 3A, anti-FAP-IL) only very weak interaction was observed with control liposomes (Fig. 3A, Cys-Lip) and with the anti-FAP-IL when competing with 10 μg of free FAP-specific scFv′ (Fig. 3A, anti-FAP-IL + free scFv′FAP). Furthermore, the anti-FAP-IL did not bind to various eukaryotic FAP-negative cell lines, for example the human breast adenocarcinoma cell line SKBR3, the mouse melanoma cell line B16F10, and the human embryonic kidney cell line HEK293, whereas only weak interaction could be observed with human umbilical vein endothelial cells, HUVEC (Fig. 3C).

To analyze the stability of anti-FAP-IL under physiological conditions the liposomes were incubated for 24 h with 50% human plasma or PBS at 37 °C. Here, anti-FAP-IL was labeled with the red fluorescent membrane probe DiI. Only a slightly decreased binding was observed for anti-FAP-IL pre-incubated with human plasma compared to anti-FAP-IL pre-incubated with PBS (Fig. 3B). Anti-FAP-IL pre-incubated with 50% human plasma or PBS for up to 72 h (Supporting Information S5) revealed distinctive binding to FAP-expressing cells.

To confirm binding and uptake of the anti-FAP-ILs, monolayer cultures of different FAP-expressing and FAP-negative cell lines were grown on cover slips and analyzed by confocal laser scanning microscopy after incubation with the liposomes (Fig. 3D). Anti-FAP-IL could be taken up exclusively by FAP-expressing cells which was evident in a high uptake by the stably transfected human fibrosarcoma HT1080-hFAP cell line and the melanoma cell line MDA-MB-435S with low endogenous FAP expression (Fig. 3D, 37 °C). Opposed to this, the wild-type human fibrosarcoma cell line HT1080 incubated with the liposomes for 8 h revealed no uptake of the liposomes (Fig. 3D, HT1080-wt). In order to verify whether the anti-FAP-IL is taken up actively by receptor-mediated internalization, HT1080-hFAP cells were incubated for 6 h at 4 °C immediately after addition of liposomes. Confocal microscopy of the cells revealed specific binding of the anti-FAP-IL to the cell membrane (Fig. 3D, 4 °C). A diffuse intracellular NIR-fluorescence of DY-676-COOH (red fluorescence) was observed, which differs from the intracellular fluorescence caused by internalized liposomes at 37 °C. The difference is a vesicular localization (Fig. 3D, 37 °C) versus diffuse NIR fluorescence due to membrane fusion and release of dye into the cytosol (Fig. 3D, 4 °C). The non-targeted Cys-Lip revealed no uptake by wild-type or FAP-expressing cell lines (Fig. 3D, Cys-Lip), which indicates that uptake of the anti-FAP-IL is specifically mediated by the FAP protein expressed on the cell surface.

4.4. Whole body in vivo optical imaging of human fibrosarcoma and melanoma in mice xenograft models

A gradual and persistent increase in the fluorescence of tumors could be detected 2 to 24 h post-intravenous injection of the anti-FAP-IL (Fig. 4). After 24 h there was a gradual decrease in the fluorescence intensity with time. However, there was still a strong fluorescence signal in the tumors 48 h post injection. The targeted anti-FAP-IL revealed distinct uptake by the different tumor models with especially high accumulations in both the HT1080-wt and HT1080-hFAP-derived xenograft models. Consistent with the specific receptor-mediated accumulation of anti-FAP-IL in high FAP-expressing tumors, competitive blocking by co-injection of the anti-FAP-IL together with 10 μg of soluble scFv′FAP resulted in significantly lower fluorescence intensities of tumors from 6 to 48 h p.i. (Fig. 4A and D, anti-FAP-IL/block). Furthermore, injection of the non-targeted liposome (Cys-Lip) in mice bearing the FAP-transfected HT1080-hFAP xenografts resulted in lower fluorescence intensities of tumors from 10 to 48 h p.i., compared to mice which received the anti-FAP-IL (Fig. 4A and D, Cys-Lip). Opposed to these observations, competitive blocking by co-injection of the anti-FAP-IL together with 10 μg of soluble scFv′FAP in mice bearing the wild-type HT1080 xenografts resulted in significant decrease in fluorescence signals only at 10 to 28 h p.i. (Fig. 4B and D, anti-FAP-IL/block) compared to those injected with anti-FAP-IL alone (Fig. 4B and D, anti-FAP-IL). We further verified whether anti-FAP-IL will accumulate in xenografts of the human melanoma cell line MDA-MB435S which has very low endogenous expression of FAP protein (Supporting Information S1). The MDA-MB435S melanoma cell line produced only small xenografts with 32 mm^3 mean volume 3–8 weeks post implantation of 2×10^6 cells. Despite the small size of the melanoma tumor models, accumulation of the anti-FAP-IL could be monitored, which could be minimally reduced by competitive blocking with soluble scFv′FAP (Fig. 4C and D).

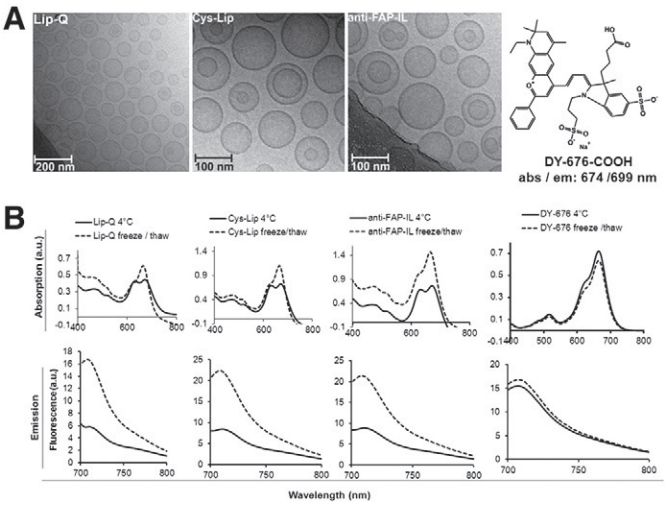

Fig. 2. A.) Representative cryo-transmission electron micrographs of liposomes prior to (Lip-Q) and post insertion of Ligand-MalPEG$_{2000}$-DSPE micelles (cysteine as control, Cys-Lip and scFv′FAP (anti-FAP-IL)) and the structure of encapsulated DY-676-COOH. B.) Absorption and emission spectra of activatable liposomes before and after rupturing by freeze and thaw treatment which reveals the release and activation of the dye and an increase in fluorescence signal. For more information see [32].

4.5. Ex vivo imaging of tumors reveal insights into liposomal uptake patterns

With respect to the different tumor models, the targeted anti-FAP-IL revealed distinct accumulation patterns in the excised tumors. NIRF images of the tumor cross-sections revealed high fluorescence of anti-FAP-IL in solid tumor regions (Fig. 5A), whereas competitive blocking by co-injection of the anti-FAP-IL together with 10 μg of soluble scFv′FAP resulted in accumulation of the liposomes predominantly in the central tumor regions (Fig. 5B), which implies their activation predominantly by macrophages localized in this region. Consistent with this, tumors extracted from mice 48 h post injection of the non-targeted Cys-Lip revealed fluorescence essentially in the central necrotic regions which are characterized by a high level of macrophages (Fig. 5C).

4.6. Histological analysis of xenograft models 24 h post injection of anti-FAP-IL

To substantiate the uptake and fluorescence activation of anti-FAP-IL *in vivo*, mice were sacrificed 24 h post injection with anti-FAP-IL or Cys-Lip. Then the tumors were excised and analyzed for the presence of liposomal fluorescence. Alpha smooth muscle actin (αSMA), which serves as a marker of tumor stromal myofibroblasts was stained in order to reassure a possible colocalization of liposomal red fluorescence with this cell subset. Whereas the tumor cells of HT1080-hFAP and MDA-MB435S derived xenografts revealed strong red fluorescence of the liposomal dye (Fig. 6A, yellow arrows), the wild-type HT1080-wt derived xenografts revealed only a few red dots of the liposomal fluorescence, which partly are localized close to myofibroblasts (Fig. 6A, white arrows). Opposed to this, HT1080-hFAP derived xenografts from mice injected with the control Cys-Lip showed no red fluorescence even in the myofibroblasts (Fig. 6B, white arrow), which indicates that the anti-FAP-IL uptake and activation *in vivo* is predominantly mediated by the presence of FAP and to some extent by tumor stromal cells.

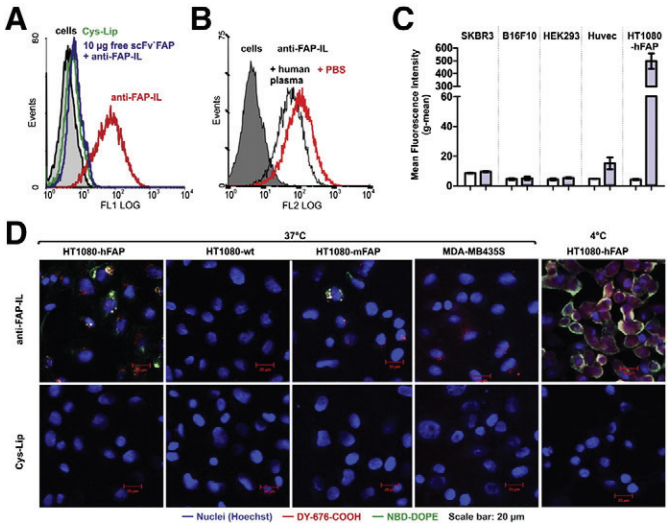

Fig. 3. Receptor-mediated uptake of anti-FAP-IL by FAP-expressing cancer cells. A.) Flow cytometric analysis of FAP-transfected cell line HT1080-mFAP incubated with 496 μM (lipid concentration) of liposomes for 1 h at 4 °C. B.) Plasma stability of anti-FAP-IL. HT1080-mFAP cells were incubated with 666 μM (lipid concentration) of liposomes which were pre-treated for 24 h at 37 °C with human plasma or PBS, then analyzed by flow cytometry. C.) Interaction of anti-FAP-IL with control cells and HT1080-hFAP. 850 μM (lipid concentration), incubated for 1 h at 4 °C, $n = 2$, non-treated cells (white), cells incubated with anti-FAP-IL (gray). D.) The wild type (HT1080-wt), the stable FAP-transfected human fibrosarcoma cell lines (HT1080-hFAP and HT1080-mFAP) as well as the endogenous FAP-expressing human melanoma cell line (MDA-MB435S) were incubated with 200 nmol of anti-FAP-IL or non-targeted liposomes (Cys-Lip) for 8 h at 37 °C or 6 h at 4 °C then imaged by confocal laser scanning microscopy.

4.7. In vitro and in vivo properties of scFv′FAP-DY-676 compared to anti-FAP-IL

scFv′FAP that was covalently coupled to DY-676-maleimide (scFv′FAP-DY-676) revealed specific binding and uptake in HT1080-hFAP cells (Fig. 7 A and B) but not the wild type cell line HT1080-wt (Supporting information S2). With reference to semi-quantitative analysis of the fluorescence intensities of cell pellets (Fig. 7A), time-course investigation of scFv′FAP-DY-676 uptake revealed rapid uptake which peaked at 8 h post application and dropped drastically after 24 h incubation. Compared to this the anti-FAP-IL revealed a gradual and persistent increase in fluorescence intensities of the cells till 24 h. Confocal microscopy revealed vesicular localization of the free scFv′FAP-DY-676 after 4 h incubation and a mixture of vesicular and predominant accumulation of the scFv′FAP-DY-676 on the membrane after 8 h and 12 h incubation (Fig. 7B, scFv′FAP-DY-676 pink arrows). This indicates a possible recycling of the scFv′FAP-DY-676 back to the cell membrane and their release out of the cells leading to lower fluorescence after 24 h incubation. Opposed to this, the anti-FAP-IL is taken up gradually and seen as vesicular localized green, red or yellow fluorescence within the cells after 4–8 h incubation (Fig. 7B, anti-FAP-IL). From 12 h incubation and higher, the green phospholipid of the anti-FAP-IL is recycled to the cell membrane whereas the NIRF dye, DY-676-COOH remains within the cells in vesicles.

Intravenous injection of scFv′FAP-DY-676, led to a fast, high contrast of the body and excretory organs such as the stomach and kidneys which interferes with detection of the tumors (Fig. 7C, whole animals). When the organs were covered with a thin black paper, imaging led to detection of contrast in tumors which was not much higher compared to the background contrast, but which however persisted in the tumors till 48 h post injection. Only a slight increase was seen at 2 h p.i. followed by rapid washout of the probes. Semi-quantitative analysis substantiates the rapid perfusion at $t = 0$–2 h p.i. and the fast washout soon after (Fig. 7D). Furthermore, it reveals that a small amount of the probe remains in both the HT1080-wt and the HT1080-hFAP tumors due to binding and EPR-effect. However, the tumors to background ratios were low (≤ 2), making the free scFv′FAP-DY-676 not suitable for imaging.

5. Discussion

The liposomes prepared in this study exhibited a narrow size distribution and were mostly unilamellarly shaped and only few bilamellar liposomes were found. Basically, the few intravesicular compartments were expected not to interfere in terms of DY-676-COOH encapsulation as well as binding of anti-FAP-IL to target cells. Supposing the bilamellar structures arise during liposome preparation and before post-insertion and being similar for both formulations (Lip-Q and anti-FAP-IL). Furthermore, a minor negative zeta-potential was measured. The post-insertion process and two separate gel filtration and ultracentrifugation steps during immunoliposome preparation did not affect the liposomal morphology, as confirmed by cryo-transmission electron microscopy. The immunoliposomes produced in this study were similar to DY-676-COOH containing liposomes (Lip-Q) which were not centrifuged and passed a gel filtration column only once [32]. Furthermore, the anti-FAP-IL and Cys-Lip formulations revealed quenching and fluorescence activation property *in vitro*, similar to Lip-Q, implying that their application in *in vivo* studies would reduce the background signals during blood circulation and enhance NIRF signal detection of targets exclusively upon cellular uptake and lysosomal processing, which result in liposomal degradation and fluorescence activation.

ScFv′FAP is cross reactive and known for the specific interaction with human and murine FAP-expressing cells [16,36]. Murine FAP (mFAP) and human FAP (hFAP) share up to 89% amino acid homology and the same structural features [36]. Therefore, both cell lines (HT108-hFAP and HT1080-mFAP) can be used for *in vitro* or *in vivo* binding studies.

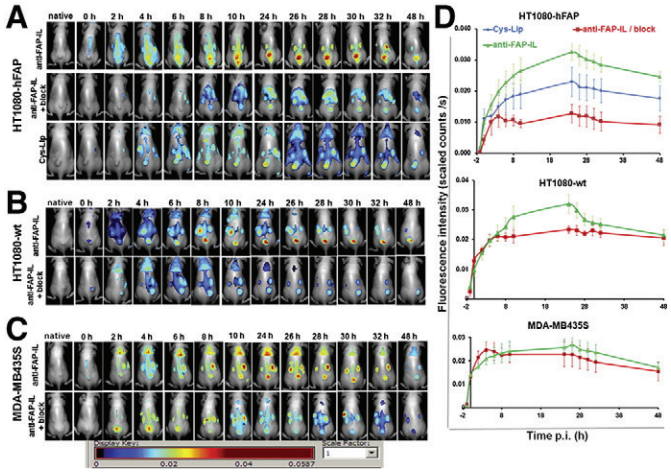

Fig. 4. Representative *in vivo* NIR-fluorescence images of mice bearing human xenograft models. A.) FAP-transfected fibrosarcoma (HT1080-hFAP, $n = 8$ without block, $n = 4$ with block, $n = 6$ with Cys-Lip). B.) Fibrosarcoma (HT1080-wt, $n = 8$ without block, $n = 4$ with block) and C.) Melanoma (MDA-MB435S, $n = 5$ without block, $n = 4$ with block) D.) Semi-quantitative analysis of fluorescence intensities of tumors at the given time points post probe injection. Each point represents the mean of fluorescence intensities of $n = 4$–8 mice ± SEM.

Binding of free soluble scFv`FAP to mFAP and hFAP-expressing cells revealed a high affinity EC_{50} of 3.8 nM and 1.7 nM respectively [36]. The successful preparation of anti-FAP targeted immunoliposomes was already shown for two different immunoliposomal preparation techniques, by the post-insertion [17,18] and by the conventional coupling technique [16]. Both methods can be used for the successful generation of specific interacting, plasma stable anti-FAP targeted immunoliposomes.

The slight influence exerted by plasma on the binding property of anti-FAP-IL in *in vitro* tests did not hamper a specific targeting to FAP-expressing cells in *in vivo* applications. The slight modulations of the binding properties might be the result of interactions of plasma proteins with anti-FAP-IL despite their PEGylation of 5 mol.%. Inactivation of scFv′FAP by thermal triggers during preparation can be excluded because scFv′FAP exhibits a protein melting point of 56 °C (not shown) and could withstand the post-insertion process carried out at 50 °C. Confocal laser scanning microscopic investigations revealed a specific active uptake of anti-FAP-IL by FAP-expressing cells and their localization in vesicles. Consistent with this, the melanoma cell line MDA-MB435S with low endogenous expression of FAP protein (see Supporting Information S1) revealed low liposomal uptake and as such only weak fluorescence signals which, however, was characterized by vesicular localization. The vesicular localization of liposomal fluorescence is in agreement with literature where non-activatable FAP-targeted immunoliposomes prepared via conventional coupling co-localized with the endosomal compartment after incubation with HT1080-mFAP at 37 °C [16]. Interestingly, cells which were incubated with anti-FAP-IL at 4 °C for 6 h showed a massive green or yellow stained cell membrane, with a slight, diffuse intracellular red fluorescence in the cytoplasm. Due to double labeling (DY-676-COOH, red and NBD-DOPE, green) of anti-FAP-IL, intact fluorescence-quenched liposomes appear green. Taking this into account, the green staining of cell membranes suggests that anti-FAP-IL binds to the cell surface at 4 °C but does not enter the cell via an active uptake mechanism. It is likely that liposomal fusion takes place with cell membranes; thus, part of the liposomal encapsulated DY-676-COOH is released into the cytosol resulting in the diffuse yellowish and intracellular red fluorescence. However, fusion processes between liposomes and cell membranes are mainly reported for vesicles containing fusogenic compounds such as 1,2-dioleoyl-sn-glycero-3-phosphoethanolamine [37,38], lysolecithin or phosphatidylserine [39] or cationic compounds [40] which are not present in the underlying anti-FAP-IL. Whether the stability of the liposomes is affected under the incubation conditions (6 h, 4 °C in the culture medium) is not known. However, the size and the encapsulated DY-676-COOH level and fluorescence activation of the activatable liposomes were not influenced by storage. For example, the Z-average and PDI of the fluorescence activatable liposomes remained identical (<1% difference) after 15 months of storage at 4 °C indicating that the liposomes are still intact and stable under these storage conditions. Furthermore, anti-FAP-IL pre-incubated for 72 h with 50% human plasma at 37 °C retained binding to FAP-expressing cells (Supporting information S5). In time-course investigations of the anti-FAP-IL versus free scFv′FAP-DY-676 uptake in HT1080-hFAP cells, recycle of the scFv′FAP-DY-676 and also of liposomal green phospholipid NBD-DOPE to the cell membrane (after liposomal degradation) could be seen, which were in accordance with earlier observations seen in macrophages where non-targeted quenched liposomes were used [32]. Thus in confocal laser scanning microscopy the fluorescence intensity of cells incubated with anti-FAP-IL at 4 °C appeared more intensive due to "accumulation" at cell surface compared to cells incubated with anti-FAP-IL at 37 °C where all uptake and recycling processes are active.

Owing to fluorescence quenching of the anti-FAP-IL, high fluorescence signals can only be measured after their degradation and resulting release and activation of the encapsulated NIR fluorescent dye. Specific activation of the anti-FAP-IL in *in vivo* xenograft models was characterized by intensive NIRF signals of tumors which increased with increasing duration after injection. This was substantiated by the distribution of liposomal fluorescence signals in slices of tumor sections prepared 24 h post injection of anti-FAP-IL, which opposed to Cys-Lip was found predominantly in tumor cells (see Fig. 6). Furthermore, liposomal uptake and fluorescence activation in FAP-expressing tumor models was partially suppressed, resulting in reduced fluorescence signals in tumors (tumor-to-background signals (TBR) from 6 to 3 at $t = 24$ h onwards, Supporting information S3) after simultaneous injection of anti-FAP-IL and free scFv′FAP, which both compete for target binding. This indicates the accumulation of the liposomal probe in the tumors via enhanced permeability and retention effect (EPR) [41] and their activation after their uptake predominantly by FAP-expressing cells hence successful competitive blocking in this high FAP tumor model. Considering passive accumulation of liposomes at the tumor site and liposomal degradation caused by macrophages and monocytes, only a low fluorescence signal of control liposomes (Cys-Lip) and of the FAP-negative wild type HT1080 xenografts after anti-FAP-IL injection was expected. Consistent with this, mice which received

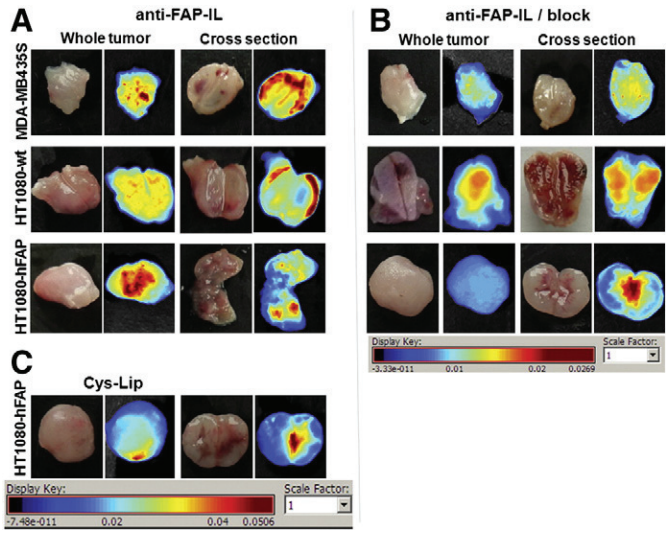

Fig. 5. *Ex vivo* NIRF images of excised xenografts. Mice implanted with the indicated tumor models were injected with A.) anti-FAP-IL, B.) anti-FAP-IL/free scFv′FAP or C.) Cys-Lip. The mice were sacrificed 48 h post injection then the tumors excised and imaged as a whole and as cross sections.

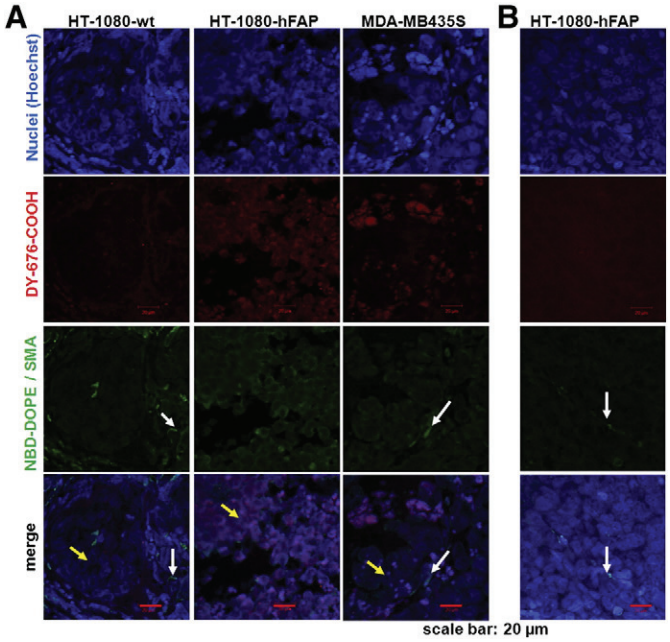

Fig. 6. Histological analysis of excised xenografts. Slices of formalin fixed paraffin-embedded tumor sections were prepared and stained for alpha-smooth muscle actin to detect myofibroblasts then imaged by confocal laser scanning microscopy. A.) Tumor sections from mice implanted with the indicated tumor models and sacrificed 24 h post injection of anti-FAP-IL. B.) Tumor sections from mice implanted with HT1080-hFAP and sacrificed 24 h post injection of the control Cys-Lip. The yellow arrows depict tumor cells whereas the white arrows point at myofibroblasts (positive for αSMA, strong green fluorescence).

Cys-Lip showed lower fluorescence signals of the HT1080-hFAP xenografts similar to the HT1080-wt xenografts. However, both control tests still permitted the detection of tumors with relatively high tumor-to-background ratios (TBR) [42] (Supporting information S3A Cys-Lip and S3B HT1080-wt). Opposed to the wild type HT1080-wt, the human melanoma with low endogenous FAP revealed lower tumor signals after application of anti-FAP-IL with TBR reaching 3 only at $t = 24$ h. Competitive blocking of anti-FAP-IL in the wild-type FAP-negative HT1080 and low FAP MDA-MB435S derived xenografts was less successful than with the high-FAP HT1080-hFAP xenografts. Whereas, only the myofibroblast subset of HT1080-wt tumors should express FAP, both the tumor cells and the myofibroblast subset in HT1080-hFAP tumor models should express high levels of FAP. The targets for free scFv′FAP are therefore readily accessible for competition between liposomes and the free scFv′FAP in the HT1080-hFAP tumor models. Furthermore, the intracellular recycling of the scFv to the cell membrane as seen with the scFv′FAP-DY-676 after 8 h and 12 h incubation on HT1080-hFAP (see Fig. 7A and B) supports the possible interference of liposomal uptake by scFv located on the cell membrane. Opposed to this, the myofibroblasts in HT1080-wt tumors are only reached by a low portion of the free scFv′FAP, resulting in less efficient competitive blocking in these tumor models since macrophages play a vital role in liposomal activation in this tumor model. As a result significant differences ($P < 0.05$) in the fluorescence intensity of competitively blocked versus non blocked counterparts in the wildtype xenografts could only be seen at time points 10–28 h post injection. Considering that the low amount of free scFv is recycled to the membrane from 8 h after uptake, it is likely that the blocking intensifies from this time point onwards. Competitive blocking in the low FAP-expressing melanoma (MDA-MB435S)-derived xenografts resulted in slight, but no significant ($P > 0.05$) decrease in fluorescence intensity which also reflects the role of stromal phagocytes in the activation of the quenched liposome in this model. Contrarily, distinct decreases in fluorescence signals of competitively blocked versus non blocked stable FAP-expressing xenografts were seen at time points 6–48 h.

From research reports, it is known that free scFv and PEGylated liposomes have varying plasma half-lives. For example, the scFvCEA molecule, a 28 kDa scFv fragment directed against human carcinoembryonic antigen (CEA) revealed a plasma half-life of $t_{1/2}\alpha = 5$ min and $t_{1/2}\beta = 4$ h [24]. Contrarily, liposomes composed of phophatidylcholine and cholesterol exhibit a plasma half-life of $t_{1/2}\beta = 13$ h and addition of sphingomyelin and 10 mol.% PEG_{1900}-DSPE increased the plasma half-life of the same formulation to $t_{1/2}\,\beta = 25$ h [43]. Despite their pharmacokinetic dependence on parameters such as liposome composition, size, charge, PEG and cholesterol amount [44,45], PEG chain length [46] and applied dose [43] it is likely that free scFv′FAP fragments are cleared more rapidly *in vivo* than anti-FAP-IL. This means that scFv′FAP fragments compete against anti-FAP-IL in the tumors only for as long as the EPR effect will permit retention of scFv. Interestingly, intravenous injection of scFv′FAP-DY-676 led to rapid clearance and insufficient detection of tumors when whole animals were imaged. However, local imaging of the regions with tumors showed accumulation and retention of a small portion of the probe within the HT1080-wt and HT1080-hFAP tumors up till 48 h p.i. This reveals that despite their low plasma half-life [23] and rapid clearance, scFv reaches the tumors by EPR effect and is retained within the tumor stroma and/or within tumor cells due to binding. The organ distribution of mice received anti-FAP-IL 48 h post injection showed high kidney and gall bladder and tumor fluorescence meaning that anti-FAP-IL would be predominantly cleared and excreted via urine and feces. Liposomes *per se* accumulate beside the target area in the tumor predominantly in organs of the mononuclear phagocyte system (former reticulo–endothelial system) as liver and spleen which are involved in the clearance of PEGylated liposomes [47]. Whether tumor associated macrophages (TAMs) play a role in the differences seen between the HT1080-wt and HT1080-hFAP tumor signals was not investigated in detail. Interestingly, Kirpotin *et al.* reported increased uptake of Fab-immunoliposomes targeting HER2 as well as non-targeted liposomes by TAMs in animal trials [48]. Furthermore, immunohistochemical staining of macrophages and fibroblasts showed dense macrophage populations in the central tumor regions and fibroblasts on the outer tumor regions (result not shown). In accordance with this, cross sections of excised tumors revealed strong fluorescence signals of the non-targeted Cys-Lip in the central regions of HT1080-hFAP-derived tumor models similar to signals of the anti-FAP-IL seen in all the investigated xenograft models following competitive blocking. Taken together, the underlying findings reveal that selective activation of the anti-FAP-IL is predominantly caused by FAP-expressing cells *in vivo*, which enables specific receptor-mediated imaging of high FAP-expressing tumor models.

However, in the absence of FAP-expressing cells, uptake and liposomal activation by tumor-associated-macrophages would also enable detection of tumors with the liposomal formulations. The use of molecular targets against FAP is advantageous over non-targeted liposomal probes due to imaging sensitivity. However, based on the underlying findings, it can be suggested that targeted liposomes would be suitable if directed delivery of dyes or drugs into tumor cells are intended, whereas the use of non-targeted liposomes would favor delivery to stromal phagocytes. Simultaneous administration of both liposome formulations would therefore be a promising approach to deliver drugs into tumor cells and stromal macrophages concomitantly. Using anti-FAP-IL as drug carrier system for drugs and diagnostics simultaneously the liposomes could be used to combine diagnosis and therapy in future.

6. Conclusion

We present a fluorescence-activatable anti-FAP-IL which targets high FAP-expressing cells for *in vivo* diagnostic imaging. The anti-FAP-IL is characterized by fluorescence quenching and specific binding to FAP-expressing target cells. This guarantees NIRF imaging exclusively

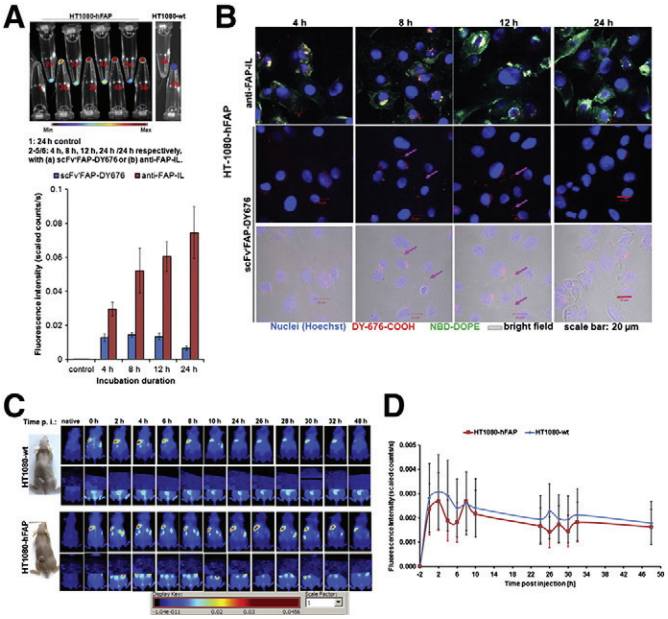

Fig. 7. *In vitro* and *in vivo* evaluation of scFv′FAP-DY-676. **A.)** NIRF images of cell pellets after incubation with 2 μg scFv′FAP-DY-676 or anti-FAP-IL (100 nmol final lipid) for 4 h, 8 h, 12 h and 24 h. The bar diagram depicts the fluorescence intensities of the cell pellets. Each bar represents the average of 2 independent experiments ± SD. B.) Corresponding confocal microscopic images to A). C.) Whole body and local (covered) NIRF images of animals bearing wt and FAP-expressing fibrosarcoma-derived xenografts after injection with scFv′FAP-DY-676. D.) Semi-quantitative analyses of ROI (tumors) at given time points post injection ($n = 5 \pm$ SEM).

after intracellular degradation of the liposomes with resulting fluorescence activation and high tumor to background ratios reaching 7 after 48 h. Targeting directs the liposomes to FAP-expressing cells whereas non-targeted liposomes are directed to stromal phagocytes. The increase in fluorescence intensity of tumors which persists up to 48 h post injection reflects the active uptake of anti-FAP-IL by tumor cells and cells of the tumor stroma, and reveals the potential of anti-FAP-IL in FAP-based diagnostic stratification of patients with superficial tumors such as breast cancers, image-guided monitoring of therapy efficacy as well as image-guided surgery. Anti-FAP-IL is therefore a valuable diagnostic tool for future stratification of patients before therapy.

Conflict of interest

The authors declare no conflict of interest.

Acknowledgments

This work was supported by the Deutsche Forschungsgemeinschaft grants HI-698/10-1 and RU-1652/1-1. We thank Susann Burgold and Julia Goering for excellent technical assistance and the company DYOMICS GmbH, Jena for their kind support.

Appendix A. Supplementary data

Supplementary data to this article can be found online at http://dx.doi.org/10.1016/j.jconrel.2014.04.050.

References

[1] W.N. Brennen, J.T. Isaacs, S.R. Denmeade, Rationale behind targeting fibroblast activation protein-expressing carcinoma-associated fibroblasts as a novel chemotherapeutic strategy, Mol. Cancer Ther. 11 (2012) 257–266.
[2] W.J. Rettig, P. Garin-Chesa, H.R. Beresford, H.F. Oettgen, M.R. Melamed, L.J. Old, Cell-surface glycoproteins of human sarcomas: differential expression in normal and malignant tissues and cultured cells, Proc. Natl. Acad. Sci. U. S. A. 85 (1988) 3110–3114.
[3] P. Garin-Chesa, L.J. Old, W.J. Rettig, Cell surface glycoprotein of reactive stromal fibroblasts as a potential antibody target in human epithelial cancers, Proc. Natl. Acad. Sci. U. S. A. 87 (1990) 7235–7239.
[4] R. Kalluri, M. Zeisberg, Fibroblasts in cancer, Nat. Rev. Cancer 6 (2006) 392–401.
[5] M.J. Scanlan, B.K. Raj, B. Calvo, P. Garin-Chesa, M.P. Sanz-Moncasi, J.H. Healey, L.J. Old, W.J. Rettig, Molecular cloning of fibroblast activation protein alpha, a member of the serine protease family selectively expressed in stromal fibroblasts of epithelial cancers, Proc. Natl. Acad. Sci. U. S. A. 91 (1994) 5657–5661.
[6] T. Kelly, Fibroblast activation protein-alpha and dipeptidyl peptidase IV (CD26): cell-surface proteases that activate cell signaling and are potential targets for cancer therapy, Drug Resist. Updat. 8 (2005) 51–58.
[7] K. Aertgeerts, I. Levin, L. Shi, G.P. Snell, A. Jennings, G.S. Prasad, Y. Zhang, M.L. Kraus, S. Salakian, V. Sridhar, R. Wijnands, M.G. Tennant, Structural and kinetic analysis of the substrate specificity of human fibroblast activation protein alpha, J. Biol. Chem. 280 (2005) 19441–19444.
[8] J.D. Cheng, R.L. Dunbrack Jr., M. Valianou, A. Rogatko, R.K. Alpaugh, L.M. Weiner, Promotion of tumor growth by murine fibroblast activation protein, a serine protease, in an animal model, Cancer Res. 62 (2002) 4767–4772.
[9] Y. Huang, A.E. Simms, A. Mazur, S. Wang, N.R. Leon, B. Jones, N. Aziz, T. Kelly, Fibroblast activation protein-alpha promotes tumor growth and invasion of breast cancer cells through non-enzymatic functions, Clin. Exp. Metastasis 28 (2011) 567–579.
[10] H.O. Lee, S.R. Mullins, J. Franco-Barraza, M. Valianou, E. Cukierman, J.D. Cheng, FAP-overexpressing fibroblasts produce an extracellular matrix that enhances invasive velocity and directionality of pancreatic cancer cells, BMC Cancer 11 (2011) 245.
[11] R.D. Hofheinz, S.E. al Batran, F. Hartmann, G. Hartung, D. Jäger, C. Renner, P. Tanswell, U. Kunz, A. Amelsberg, H. Kuthan, G. Stehle, Stromal antigen targeting by a humanised monoclonal antibody: an early phase II trial of sibrotuzumab in patients with metastatic colorectal cancer, Onkologie 26 (2003) 44–48.
[12] R. Weissleder, V. Ntziachristos, Shedding light onto live molecular targets, Nat. Med. 9 (2003) 123–128.
[13] K. Licha, B. Riefke, B. Ebert, C. Grötzinger, Cyanine dyes as contrast agents in biomedical optical imaging, Acad. Radiol. 9 (Suppl. 2) (2002) S320–S322.
[14] G.D. Luker, K.E. Luker, Optical imaging: current applications and future directions, J. Nucl. Med. 49 (2008) 1–4.
[15] G.M. van Dam, G. Themelis, L.M. Crane, N.J. Harlaar, R.G. Pleijhuis, W. Kelder, A. Sarantopoulos, J.S. de Jong, H.J. Arts, A.G. van der Zee, J. Bart, P.S. Low, V. Ntziachristos, Intraoperative tumor-specific fluorescence imaging in ovarian cancer by folate receptor-alpha targeting: first in-human results, Nat. Med. 17 (2011) 1315–1319.
[16] P. Baum, D. Müller, R. Rüger, R.E. Kontermann, Single-chain Fv immunoliposomes for the targeting of fibroblast activation protein-expressing tumor stromal cells, J. Drug Target. 15 (2007) 399–406.
[17] S.K. Messerschmidt, A. Kolbe, D. Müller, M. Knoll, J. Pleiss, R.E. Kontermann, Novel single-chain Fv′ formats for the generation of immunoliposomes by site-directed coupling, Bioconjug. Chem. 19 (2008) 362–369.
[18] S.K. Messerschmidt, A. Musyanovych, M. Altvater, P. Scheurich, K. Pfizenmaier, K. Landfester, R.E. Kontermann, Targeted lipid-coated nanoparticles: delivery of tumor necrosis factor-functionalized particles to tumor cells, J. Control. Release 137 (2009) 69–77.
[19] J. Li, K. Chen, H. Liu, K. Cheng, M. Yang, J. Zhang, J.D. Cheng, Y. Zhang, Z. Cheng, Activatable near-infrared fluorescent probe for *in vivo* imaging of fibroblast activation protein-alpha, Bioconjug. Chem. 23 (2012) 1704–1711.
[20] M. Ogawa, N. Kosaka, P.L. Choyke, H. Kobayashi, *In vivo* molecular imaging of cancer with a quenching near-infrared fluorescent probe using conjugates of monoclonal antibodies and indocyanine green, Cancer Res. 69 (2009) 1268–1272.
[21] M. Ogawa, C.A. Regino, P.L. Choyke, H. Kobayashi, *In vivo* target-specific activatable near-infrared optical labeling of humanized monoclonal antibodies, Mol. Cancer Ther. 8 (2009) 232–239.
[22] G.T. Hermanson, Bioconjugate Techniques, Elsevier Science, 2010.
[23] R. Stork, K.A. Zettlitz, D. Müller, M. Rether, F.G. Hanisch, R.E. Kontermann, N-glycosylation as novel strategy to improve pharmacokinetic properties of bispecific single-chain diabodies, J. Biol. Chem. 283 (2008) 7804–7812.
[24] D. Müller, A. Karle, B. Meissburger, I. Höfig, R. Stork, R.E. Kontermann, Improved pharmacokinetics of recombinant bispecific antibody molecules by fusion to human serum albumin, J. Biol. Chem. 282 (2007) 12650–12660.
[25] J. Buse, A. El-Aneed, Properties, engineering and applications of lipid-based nanoparticle drug-delivery systems: current research and advances, Nanomedicine (Lond) 5 (2010) 1237–1260.
[26] Y. Malam, M. Loizidou, A.M. Seifalian, Liposomes and nanoparticles: nanosized vehicles for drug delivery in cancer, Trends Pharmacol. Sci. 30 (2009) 592–599.
[27] M.A. Dobrovolskaia, S.E. McNeil, Immunological properties of engineered nanomaterials, Nat. Nanotechnol. 2 (2007) 469–478.
[28] M.A. Dobrovolskaia, S.E. McNeil, Understanding the correlation between *in vitro* and *in vivo* immunotoxicity tests for nanomedicines, J. Control. Release 172 (2013) 456–466.
[29] J. Szebeni, Complement activation-related pseudoallergy: a new class of drug-induced acute immune toxicity, Toxicology 216 (2005) 106–121.
[30] J. Szebeni, P. Bedocs, D. Csukas, L. Rosivall, R. Bunger, R. Urbanics, A porcine model of complement-mediated infusion reactions to drug carrier nanosystems and other medicines, Adv. Drug Deliv. Rev. 64 (2012) 1706–1716.
[31] J. Szebeni, P. Bedocs, R. Urbanics, R. Bunger, L. Rosivall, M. Toth, Y. Barenholz, Prevention of infusion reactions to PEGylated liposomal doxorubicin via tachyphylaxis induction by placebo vesicles: a porcine model, J. Control. Release 160 (2012) 382–387.
[32] F.L. Tansi, R. Rüger, M. Rabenhold, F. Steiniger, A. Fahr, W.A. Kaiser, I. Hilger, Liposomal Encapsulation of a Near-Infrared Fluorophore Enhances Fluorescence

Quenching and Reliable Whole Body Optical Imaging Upon Activation *In Vivo*, Small 9 (21) (2013 Nov 11) 3659–3669.
[33] S.J. Thorpe, C. Turner, A. Heath, I. Feavers, I. Vatn, J.B. Natvig, K.M. Thompson, Clonal analysis of a human antimouse antibody (HAMA) response, Scand. J. Immunol. 57 (2003) 85–92.
[34] R. Rüger, D. Müller, A. Fahr, R.E. Kontermann, Generation of immunoliposomes using recombinant single-chain Fv fragments bound to Ni-NTA-liposomes, J. Drug Target. 13 (2005) 399–406.
[35] K. Mack, R. Rüger, S. Fellermeier, O. Seifert, R.E. Kontermann, Dual targeting of tumor cells with bispecific single-chain Fv-immunoliposomes, Antibodies 1 (2012) 199–214.
[36] B. Brocks, P. Garin-Chesa, E. Behrle, J.E. Park, W.J. Rettig, K. Pfizenmaier, D. Moosmayer, Species-crossreactive scFv against the tumor stroma marker "fibroblast activation protein" selected by phage display from an immunized $FAP^{-/-}$ knock-out mouse, Mol. Med. 7 (2001) 461–469.
[37] N. Düzgünes, J. Wilschut, R. Fraley, D. Papahadjopoulos, Studies on the mechanism of membrane fusion. Role of head-group composition in calcium- and magnesium-induced fusion of mixed phospholipid vesicles, Biochim. Biophys. Acta 642 (1981) 182–195.
[38] R. Sundler, N. Düzgünes, D. Papahadjopoulos, Control of membrane fusion by phospholipid head groups. II. The role of phosphatidylethanolamine in mixtures with phosphatidate and phosphatidylinositol, Biochim. Biophys. Acta 649 (1981) 751–758.
[39] R.R.C. New, Liposomes: A Practical Approach, IRL Press at Oxford University Press, Oxford, 1990.
[40] P.L. Felgner, T.R. Gadek, M. Holm, R. Roman, H.W. Chan, M. Wenz, J.P. Northrop, G.M. Ringold, M. Danielsen, Lipofection: a highly efficient, lipid-mediated DNA-transfection procedure, Proc. Natl. Acad. Sci. U. S. A. 84 (1987) 7413–7417.
[41] T.A. ElBayoumi, V.P. Torchilin, Tumor-targeted nanomedicines: enhanced antitumor efficacy *in vivo* of doxorubicin-loaded, long-circulating liposomes modified with cancer-specific monoclonal antibody, Clin. Cancer Res. 15 (2009) 1973–1980.
[42] J. Cao, S. Wan, J. Tian, S. Li, D. Deng, Z. Qian, Y. Gu, Fast clearing RGD-based near-infrared fluorescent probes for *in vivo* tumor diagnosis, Contrast Media Mol. Imaging 7 (2012) 390–402.
[43] T.M. Allen, C. Hansen, Pharmacokinetics of stealth versus conventional liposomes: effect of dose, Biochim. Biophys. Acta 1068 (1991) 133–141.
[44] D.D. Lasic, D. Papahadjopoulos, Liposomes revisited, Science 267 (1995) 1275–1276.
[45] J. Senior, J.C. Crawley, G. Gregoriadis, Tissue distribution of liposomes exhibiting long half-lives in the circulation after intravenous injection, Biochim. Biophys. Acta 839 (1985) 1–8.
[46] K. Maruyama, T. Yuda, A. Okamoto, S. Kojima, A. Suginaka, M. Iwatsuru, Prolonged circulation time *in vivo* of large unilamellar liposomes composed of distearoyl phosphatidylcholine and cholesterol containing amphipathic poly(ethylene glycol), Biochim. Biophys. Acta 1128 (1992) 44–49.
[47] T. Lammers, S. Aime, W.E. Hennink, G. Storm, F. Kiessling, Theranostic nanomedicine, Acc. Chem. Res. 44 (2011) 1029–1038.
[48] D.B. Kirpotin, D.C. Drummond, Y. Shao, M.R. Shalaby, K. Hong, U.B. Nielsen, J.D. Marks, C.C. Benz, J.W. Park, Antibody targeting of long-circulating lipidic nanoparticles does not increase tumor localization but does increase internalization in animal models, Cancer Res. 66 (2006) 6732–6740.